

NUMERICAL SIMULATION STUDY ON ROCK BREAKAGE BY LOW TEMPERATURE JET IMPACT

by

Hu WANG^a, Yong HU^{a*}, Cheng-Zheng CAI^b, Bo WANG^b, and Yi LYV^b

^aXinjiang Yaxin Coalbed Methane Investment and Development (Group) Co., Ltd., Urumqi, China

^bState key Laboratory of Intelligent Construction and Healthy Operation and Maintenance of Deep Underground Engineering, China University of Mining and Technology, Xuzhou, China

Original scientific paper

<https://doi.org/10.2298/TSCI2502503W>

A 3-D model with specific parameters was established, utilizing the conjugate heat transfer method to calculate heat exchange between the rock and fluid, and the smoothed particle hydrodynamics-finite element method approach to simulate rock fragmentation. Upon contact, the liquid nitrogen jet induced significant heat exchange, with the 25 MPa jet showing larger contact area and higher efficiency. Notably, the impact center of the 400 °C rock exhibited a slight temperature rise due to energy release. Liquid nitrogen reduced the rock's tensile, compressive strengths, and elastic modulus. High temperature rocks (400 °C) had a 15.8% higher eroded volume fraction than those at 200 °C. Increasing jet pressure from 20-25 MPa resulted in a 32.0% erosion increase. Additionally, a decrease in elastic modulus for 200 °C granite led to a 19.9% increase in erosion.

Key words: rock fragmentation, liquid nitrogen, jet impact, flow and heat transfer

Introduction

Concurrently, environmental awareness has driven the world to explore clean energy sources. Hot dry rock (HDR), abundant and largely untapped, stands out as a promising option. HDR is a low permeability rock mass found deep underground, with temperatures exceeding 180 °C. The HDR exploitation is crucial for improving energy structures and mitigating environmental impacts [1, 2]. Traditional drilling methods, however, face challenges such as high water usage, pollution, and inefficacy in low porosity reservoirs [3]. This has led to a focus on waterless or low water technologies. Liquid nitrogen, a cryogenic fluid commonly used in industry, offers several advantages for HDR extraction [4]. It induces thermal stress in rocks, enhancing fragmentation efficiency, improves heat extraction by facilitating better contact between cold water and HDR, and addresses issues like drilling fluid intolerance to high temperatures and well leakage. In summary, liquid nitrogen jet technology presents a novel approach to HDR exploitation, potentially overcoming the limitations of traditional methods and enabling efficient, environmentally friendly development of HDR resources [5, 6].

Numerical model for rock-breaking

Heat transfer model

To gain a clearer and more intuitive understanding of the distribution of stress and temperature fields within a granite rock during jet impact, a model of liquid nitrogen jet impact-

* Corresponding author, e-mail: huyongyaxin@aliyun.com

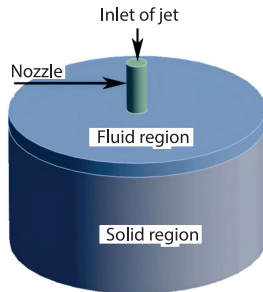


Figure 1. Geometric model of heat transfer

ing granite in a 3-D space was established. The geometric model is shown in fig. 1. During the modelling process, specific parameters were set the diameter of the granite model was 50 mm, the height was 25 mm, the jet standoff distance was 3 mm, the length of the nozzle was 10 mm, and the jet inlet diameter was 4 mm.

In the liquid nitrogen jet impacting granite process, the liquid enters through the inlet, exits beneath the nozzle to strike the rock surface, and then flows out through the upper fluid domain and annular wall. The simulation set-up comprises:

A pressure inlet at the jet inlet with the pressure is determined by operating conditions. The upper surface and sidewalls of the fluid domain are set to atmospheric pressure outlets. Stationary walls with zero velocity at the rock's lower surface and the nozzle wall.

An ideal adiabatic nozzle wall was assumed, while the rock sidewalls and bottom adhere to experimental conditions with no heat supply or flux. The conjugate heat transfer method calculates heat transfer between the rock's upper surface and the fluid domain, coupling fluid conservation equations near the wall with the solid's heat conduction equation, ensuring consistent heat flux at the interface. Governing equations for this process are provided [7]:

$$q_w|_{\text{solid}} = q_w|_{\text{fluid}} \quad (1)$$

$$-K \left(\frac{\partial T_s}{\partial n} \right) \Big|_{\text{solid}} = K_h (T_w - T_{\text{adj}}) \Big|_{\text{fluid}}$$

$$K \nabla^2 T_s = c_s \rho_s \frac{\partial T_s}{\partial t} \quad (2)$$

where K is the thermal conductivity of granite, T_s – the temperature of granite, c_s – the specific heat capacity of granite, ρ_s – the density of granite, q_w – the heat flux at the fluid-solid interface, K_h – the convective heat transfer coefficient of the fluid, T_w – the temperature of the rock wall, and T_{adj} – the temperature of the fluid near the wall.

The k - ε model is adopted for the liquid nitrogen jet. At the beginning of the calculations, the gravity coefficient is set to 9.81 m/s², and the initial state of the fluid domain and nozzle is air at 22 °C. For jets with different injection pressures, the pressures are set to 20 MPa and 25 MPa, respectively, with an initial rock temperature of 200 °C. For rocks with different initial temperatures, the initial temperatures are set to 200 °C and 400 °C, respectively.

The material model parameters for the rock are presented in tab. 1.

Table 1. Model parameters

Parameter	Jet temperature [°C]	Rock density [kgm ⁻³]	Isobaric specific heat capacity of rock [J(kg ⁻¹ K ⁻¹)]	Thermal conductivity of rock [Wm ⁻¹ K ⁻¹]
Value	-196	2780.2	2500	2.65

Rock-breaking model

The geometric model for simulating rock fragmentation is shown in fig. 2. When constructing the model, the influence of air was neglected, retaining only the jet and the rock. The model was developed using a combined smoothed particle hydrodynamics-finite element method (SPH-FEM) coupling approach. The jet was simplified as a cylinder, with its diameter and the size of the rock matrix consistent with those used in the heat transfer model. The jet

was converted into dynamic particles (SPH), while the rock matrix retained FEM elements.

In the model, the gravity coefficient was set to 9.81 m/s², with the jet directed vertically downwards. The granite was constrained to be in a fixed state, *i.e.*, the lower boundary was set as a fixed boundary condition, $u_x = 0$, $u_y = 0$, meanwhile, the upper, left, and right boundaries of the granite were set as free boundaries, $\sigma_x = 0$, $\tau_{xy} = 0$, $\sigma_y = 0$, and $\tau_{yx} = 0$.

During the calculations, liquid nitrogen was treated as a fully plastic material capable of withstanding large deformations arising from high speed impacts. The jet was modeled using the NULL constitutive model, which employs the Gruneisen equation of state to simulate the jet's behavior effectively [8]. The material model parameters for the liquid nitrogen jet are presented in the tab. 2. There is:

$$p = \frac{\rho_0 c^2 \mu \left[1 + \left(1 - \frac{\gamma_0}{2} \mu \right) - \frac{a}{2} \mu^2 \right]}{\left[1 - (S_1 - 1)\mu - S_2 \frac{\mu^2}{\mu + 1} - S_3 \frac{\mu^3}{(\mu + 1)^2} \right]} + (\gamma_0 + a\mu)E \quad (3)$$

where ρ_0 is the density of the liquid, c – the intercept of the shock wave velocity (u_s)-particle velocity (u_p) curve, S_1, S_2, S_3 are the slope coefficients of the u_s - u_p curves, γ_0 – the Mie-Gruneisen constant, and a – the first-order volume correction the Mie-Gruneisen coefficient.

Table 2. Jet model parameters

Fluid	ρ_0 [kgm ⁻³]	c [ms ⁻¹]	S_1	S_2	S_3	a	γ_0
Liquid nitrogen	860	1272	2.98	-1.607	0.1829	1.512	0.39

In this simulation, the H-J-C model was adopted for the rock constitutive model. This model comprehensively considers the effects of strain rate, damage evolution, confining pressure, and crushing/compaction, enabling it to accurately describe the mechanical behavior of concrete and rock materials under large deformations, high strain rates, and high hydrostatic pressures. The JHC model is characterized by its simplicity and clear parameter definitions, and it has been widely applied in the analysis of concrete and rock-like materials subjected to strong dynamic loads such as explosions and jet impacts. The strength of the model is described using a normalized equivalent stress [9], *i.e.*:

$$\sigma^* = \left[A(1-D) + BP^{*N} \right] \left[1 + C \ln(\dot{\epsilon}^*) \right] \quad (4)$$

where $\sigma^* = \sigma/f_c$ is the characterized equivalent stress with $\sigma^* \leq S_{\max}$, S_{\max} – the maximum characterized equivalent stress that the material can achieve, σ – the actual equivalent stress, and f_c – the quasi-static uniaxial compressive strength. The $P = p/f_c$ is the characterized pressure, and p – the hydrostatic pressure within the element. The $\dot{\epsilon}^* = \dot{\epsilon}/\dot{\epsilon}_0$ is the characterized strain rate, where $\dot{\epsilon}$ is the actual strain rate and $\dot{\epsilon}_0$ – the reference strain rate, C – the strain rate effect parameter, while A, B, N , and S_{\max} are collectively referred to as the limit surface parameters, where A – the characterized viscous strength coefficient, B – the characterized pressure hardness coefficient, and N – the pressure hardening exponent.

The damage factor D was obtained through the accumulation of equivalent plastic strain and plastic volumetric strain, and is expressed:

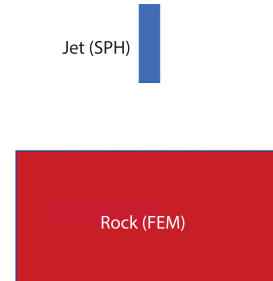


Figure 2. A geometric model of rock-breaking

$$D = \sum \frac{\Delta \varepsilon_p + \Delta \mu_p}{D_1 (P^* + T_e^*)^{D_2}} \quad (5)$$

where $\Delta \varepsilon_p$ is the incremental equivalent plastic strain, $\Delta \mu_p$ – the incremental equivalent volumetric strain, T_e^* – the normalized tensile strength, $T_e^* = T_e/f_c$, T_e – the tensile strength of the material, and D_1 and D_2 are damage constants of the material.

The granite model parameters are presented in tab. 3.

Table 3. Granite model parameters

ρ_0 [kgm ⁻³]	Shear modulus, G [GPa]	f_c [GPa]	A	B	C
2780.2	20.8	0.119	0.29	2.06	0.0013
D_2	T [GPa]	S_{\max}	N	D_1	
1	0.0082	5.0	0.866	0.04	

Rock temperature distribution

Figures 3 and 4 show the temperature contours of a rock surface under jet impacts at 20 MPa and 25 MPa. At 60 μ s, both jets contacted the rock, initiating significant heat exchange due to the temperature difference. Higher flow velocities prevented complete liquid nitrogen coverage. The 25 MPa jet, with a larger contact area, enhanced heat transfer, showing a broader influence and better cooling at 90 μ s and 120 μ s compared to the 20 MPa jet. Figure 5 displays temperature contours of a rock initially heated to 400 °C under a 20 MPa jet. An interesting observation was a slight temperature increase at the impact center, attributed to compressive and thermal deformation releasing energy. Overall, liquid nitrogen jet impacts altered rock surface temperatures, influencing subsequent fragmentation. Temperature distribution variations underscore the complex interactions between jet pressure, flow velocity, and rock's initial temperature in the fragmentation process.

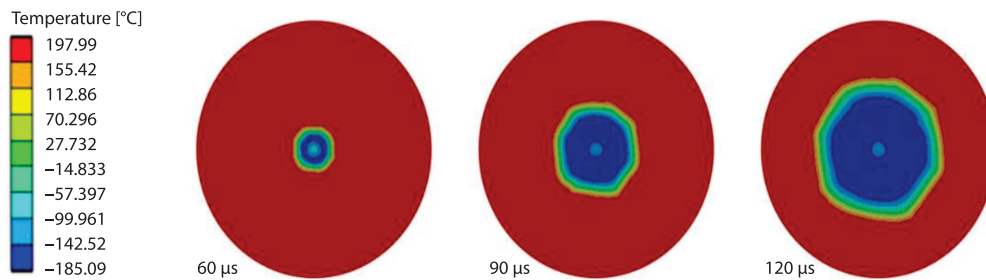


Figure 3. The surface temperature distribution for 200 °C rock impacted by a 20 MPa liquid nitrogen jet

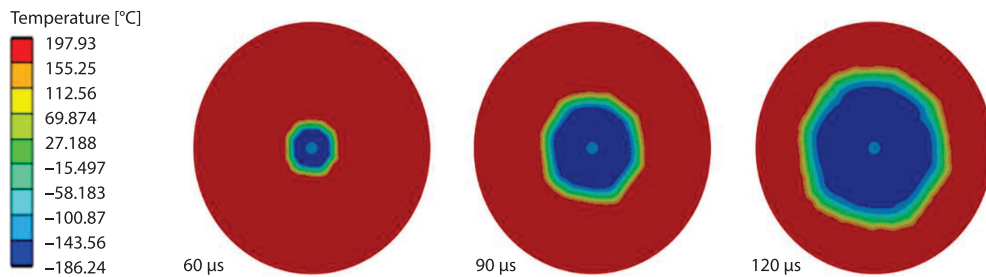


Figure 4. The surface temperature distribution for 200 °C rock impacted by a 25 MPa liquid nitrogen jet

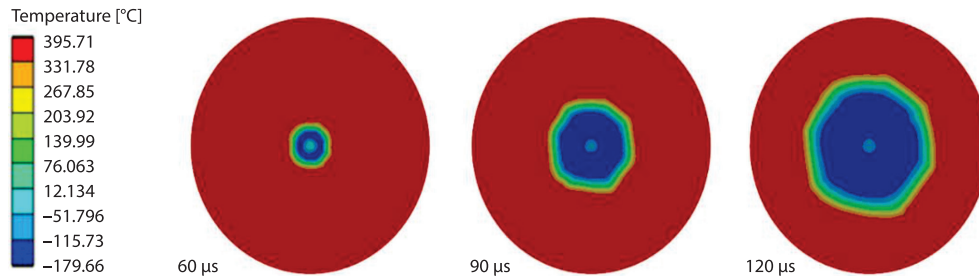


Figure 5. The surface temperature distribution for 400 °C rock impacted by a 20 MPa liquid nitrogen jet

Liquid nitrogen jet rock breaking effect

The rock in the rock-breaking simulation was degraded. For granite with an initial temperature of 200 °C, its tensile strength was assumed to be reduced by 12.5%, compressive strength by 22.6%, and elastic modulus by 11.4%. For granite with an initial temperature of 400 °C, its tensile strength was reduced by 38.5%, compressive strength by 20.6%, and elastic modulus by 20.8%.

To measure jet-induced rock damage, the eroded volume fraction—the ratio of broken to original rock volume—was introduced. Study results show that rocks with higher initial temperatures suffer greater property degradation, leading to increased erosion under identical jet pressures. For example, rocks at 400 °C had a 15.8% higher eroded volume fraction than those at 200 °C, fig. 6(a). This temperature-dependent erosion is linked to reduced elastic modulus, which correlates with lower tensile and shear strengths. Additionally, increasing jet pressure from 20-25 MPa resulted in a 32.0% increase in eroded volume fraction, fig. 6(b), highlighting the direct link between jet pressure and erosion. Simulations further explored the impact of elastic modulus on rock-breaking. When granite’s elastic modulus at 200 °C was reduced to 32 GPa from 41 GPa, with the eroded volume fraction increasing by 19.9% at 120 μs, fig. 6(c). These findings emphasize the crucial role of elastic modulus in determining erosion extent and jet efficiency. In conclusion, liquid nitrogen’s low temperature effect, along with jet pressure and initial rock temperature variations, significantly influences rock mechanics and erosion susceptibility. The eroded volume fraction quantifies jet effectiveness, while elastic modulus changes are pivotal in determining rock-breaking efficiency.

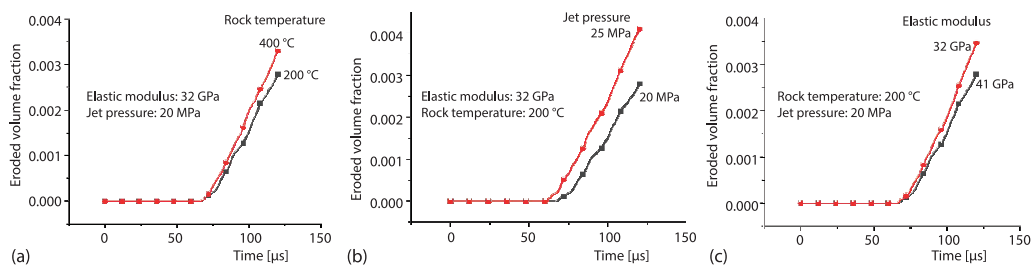


Figure 6. The volume fraction of rock fragmentation under different conditions

Conclusion

The results showed significant heat exchange upon liquid nitrogen jet contact with the rock. The 25 MPa jet had a larger contact area and higher heat transfer efficiency. A slight temperature rise at the impact center of the 400 °C rock was due to energy release from compres-

sion and thermal deformation. Liquid nitrogen reduced the rock's tensile strength, compressive strength, and elastic modulus. High temperature rocks had a higher eroded volume fraction, with the 400 °C rock showing a 15.8% increase compared to the 200 °C rock. Increasing jet pressure from 20-25 MPa raised the eroded volume fraction by 32.0%. Decreasing the elastic modulus of 200 °C granite from 41-32 GPa increased the eroded volume fraction by 19.9%.

Acknowledgment

This research was funded by the National Key R&D Program of China (Grant No. 2022YFE0129100).

Nomenclature

c_s – specific heat capacity of rock, [Jkg⁻¹K⁻¹]
 D – damage factor
 f_c – quasi-static uniaxial compressive strength, [MPa]
 K – thermal conductivity, [Wm⁻¹K⁻¹]
 q_w – heat flux, [Wm⁻²]
 P^* – characterized pressure
 p – hydrostatic pressure, [MPa]
 T – temperature, [K]
 T_{adj} – temperature of the fluid near the wall, [K]
 T_s – temperature of rock, [K]
 T_w – temperature of the rock wall, [K]

u_f – intercept of the shock wave velocity, [ms⁻¹]
 u_s – particle velocity, [ms⁻¹]

Greek symbols

γ_0 – Mie-Gruneisen constant
 $\dot{\epsilon}$ – actual strain rate, [s]
 $\dot{\epsilon}^*$ – characterized strain rate, [s]
 $\Delta\epsilon_p$ – incremental equivalent plastic strain
 $\Delta\mu_p$ – incremental equivalent volumetric strain
 ρ_s – density of rock, [kgm⁻³]
 σ – actual equivalent stress, [MPa]
 σ^* – characterized equivalent stress

References

- [1] Feng, Z., *et al.*, Permeability Evolution of Thermally Cracked Granite with Different Grain Sizes, *Rock Mechanics and Rock Engineering*, 54 (2021), 2, pp. 1953-1967
- [2] Zeng, Y., Technical Progress and Thinking for Development of Hot Dry Rock (HDR) Geothermal Resources, *Petroleum Drilling Techniques*, 43 (2015), 2, pp. 1-7
- [3] Li, G., *et al.*, Status and Challenges of Hot Dry Rock Geothermal Resource Exploitation, *Petroleum Science Bulletin*, 7 (2022), 2, pp. 343-364
- [4] Cai, C., *et al.*, Numerical Simulation of the Flow Field Structure of Liquid Nitrogen Jet, *Thermal Science*, 23 (2019), 3, pp. 1337-1343
- [5] Huang, Z., *et al.*, Mechanism of Drilling Rate Improvement Using High-Pressure Liquid Nitrogen Jet, *Petroleum Exploration and Development*, 46 (2019), 4, pp. 810-818
- [6] Huang, Z., *et al.*, Breakage Mechanism of High-Temperature Granite By Abrasive Liquid Nitrogen Jet, *Acta Petrolel Sinica*, 41 (2020), 5, pp. 604-614
- [7] Zhang, S., *et al.*, Numerical Analysis of Transient Conjugate Heat Transfer and Thermal Stress Distribution in Geothermal Drilling with High-Pressure Liquid Nitrogen Jet, *Applied Thermal Engineering*, 129 (2018), 1, pp. 1348-1357
- [8] Mi, J., *et al.*, Numerical Simulation of Rock Breaking By Rear-Mixed Abrasive Water Jet Based on an SPH-FEM Coupling Algorithm, *Journal of Vibration and Shock*, 40 (2021), 16, pp. 132-139
- [9] Liang, S., *et al.*, Research on the Dynamic Damage Properties and Determination of the Holmquist-Johnson-Cook Model Parameters for Sandstone, *Applied Sciences*, 12 (2022), 16, 8366